Electronic Supplementary Material (ESI) for New Journal of Chemistry.


# Anion-regulated 2D amorphous binary nickel-iron nitrides for efficient water oxidation at high-current-densities

Yunfei Wei‡[a], Yifan Xu‡[ac], Hongbo Zhang[a], Jingyun Jiang*[a] and Qun Xu*[ab]

[a] School of Materials Science and Engineering, Zhengzhou University, Zhengzhou, 450001, Henan, China

[b] Henan Institute of Advanced Technology, Zhengzhou University, Zhengzhou, 450052, Henan, China

[c] School of Materials Science and Engineering, Nanyang Technological University, 639798 Singapore

‡ These authors contributed equally to this work.

*Corresponding author E-mail: qunxu@zzu.edu.cn, jiangjingyun@zzu.edu.cn

# Table of contents

**Table S2** The calculated $C_{dl}$ and $R_{ct}$ values of $NiFe_{0.05}$-N-Cl-CP, $NiFe_{0.05}$-N-$NO_3$-CP, and $NiFe_{0.05}$-N-$Cl_{0.5}(NO_3)_{0.5}$-CP.

**3. References**

# 1 Experimental Section

## 1.1 Chemicals and Materials

Polyethylene glycol (PEG) 200, barbituric acid (BA), ferric trichloride hexahydrate ($FeCl_3 \cdot 9H_2O$, ≥ 99%), nickel trichloride hexahydrate ($NiCl_2 \cdot 6H_2O$, ≥ 99%), ferric nitrate nonahydrate ($Fe(NO_3)_3 \cdot 9H_2O$, ≥ 99%), nickel nitrate hexahydrate ($Ni(NO_3)_2 \cdot 6H_2O$, ≥ 99%) and absolute ethanol were purchased from Sinopharm Chemical Reagent Co., Ltd. Potassium hydroxide (KOH, ≥ 85%) was purchased from Shanghai Aladdin Biochemical Technology Co. Ltd.. Carbon paper (CP) was purchased from Toray Industries Co. Ltd. All chemicals were used directly without further purification. Deionized water was used in all experiments.

## 1.2 Materials Fabrication

**Preparation of quaternary deep eutectic solvents**: By combining PEG 200, BA, hydrated metal chlorine/nitric acid ($MCl_x \cdot yH_2O$ or $M(NO_3)_x \cdot yH_2O$, M is Ni/Fe and Ni: Fe=95:5) were mixed at molar ratio of 12:1:1 to synthesize quaternary DESs, noted that the total molar number of $M(NO_3)_x \cdot yH_2O$ and $MCl_x \cdot yH_2O$ is 10 mmol. The specific synthesis ratio is as follows.

| **Quaternary DESs** | **Molar ratio** | | | | | |
|---|---|---|---|---|---|---|
| | **PEG** | **BA** | **$MCl_x \cdot yH_2O$-$MNO_x \cdot yH_2O$** | | | |
| | | | $NiCl_2 \cdot 6H_2O$ | $FeCl_3 \cdot 9H_2O$ | $Ni(NO_3)_2 \cdot 6H_2O$ | $Fe(NO_3)_3 \cdot 9H_2O$ |
| PEG-BA-$MCl_x \cdot yH_2O$ | 12 | 1 | 0.95 | 0.05 | 0 | 0 |
| PEG-BA-$M(NO_3)_x \cdot yH_2O$ | 12 | 1 | 0 | 0 | 0.95 | 0.05 |
| PEG-BA-$MCl_x \cdot yH_2O$/ $M(NO_3)_x \cdot yH_2O$ | 12 | 1 | 0.475 | 0.025 | 0.475 | 0.025 |

**Synthesis of 2D $NiFe_{0.05}$-N-Cl-CP:** The synthesized PEG-BA-$MCl_x \cdot yH_2O$ DES was transferred to the 100 mL Teflon-lined autoclave with the tailed carbon paper (CP) electrodes, which fixed intact and then heated in the oven at 200 °C for 2 h. After cooling down the autoclave naturally, the CPs were cleaned with deionized water several times, rinsed with ethanol, and then dried in the oven at 60 °C.

**Synthesis of 2D $NiFe_{0.05}$-N-$NO_3$-CP:** The synthesis method is the same as 2D $NiFe_{0.05}$-N-Cl-CP, but the difference is that PEG-BA-$MCl_x \cdot yH_2O$ DES is changed to PEG-BA-$M(NO_3)_x \cdot yH_2O$ DES.

**Synthesis of 2D $NiFe_{0.05}$-N-$Cl_{0.5}(NO_3)_{0.5}$-CP:** The synthesis method is the same as 2D $NiFe_{0.05}$-N-Cl-CP, but the difference is that PEG-BA-$MCl_x \cdot yH_2O$ DES is changed to PEG-BA-$MCl_x \cdot yH_2O$/$M(NO_3)_x \cdot yH_2O$ DES.

### 1.3 Characterization

Differential scanning calorimetry (DSC) was performed using a DSC200F3 (Netzsch, Germany) system at a heating rate of 5 °C $min^{-1}$. The samples were cooled down at -100 °C for 10 min. Fourier Transform Infrared Spectroscopy (FT-IR) was carried out on the FT-IR spectrometer (IR Tracer 100, Japan), ranging from 700 to 4000 $cm^{-1}$. Ultraviolet Visible spectroscopy (UV-vis) tests were performed on a UV-vis spectrometer (Cary 60 UV-vis, Agilent), ranging from 190 to 1100 nm. The mass spectrometry (MS) was operated under the specific conditions (Positive ESI spray voltage is 4.5 KV, and negative ESI spray voltage is -3.5 KV; nebulizer gas, 1.5 L $min^{-1}$; drying gas, 100 Kpa; heat block temperature, 200 ℃; CDL temperature, 200 ℃; IT Area Vacuum, $1.0\times10^{-2}$ Pa; TOF Area Vacuum, $5\times10^{-4}$ Pa). Ion accumulation time was set to 10 ms, and the detector voltage was fixed at 1.6 kV. Raman tests were performed on the Micro Raman imaging spectrometer (Soleil Nano, France).

X-ray powder diffraction (XRD) was performed on a Y-2000 X-ray diffractometer (λ-2000, λ = 1.5406 Å) at a scanning rate of 10° $min^{-1}$. Contact angle characterizations were conducted by an optical contact angle measuring device (OSA100S-T, Ningbo NB Scientific Instrument Co., Ltd., Zhejiang). Scanning electron microscope (SEM) tests were obtained on an SEM (ZEISS Auriga, Germany) at an acceleration voltage of 5 KeV. Transmission electron microscope (TEM), high-resolution TEM (HRTEM), and corresponding EDS results were performed on the TEM (JEOL JEM-F200, Japan), which was equipped with a 200 kV electric field emission gun EDS. Atomic force microscopy (AFM) experiments were performed on Bruker Dimension ICON. In the TEM and AFM tests, samples were obtained by ultrasound from the $NiFe_{0.05}$-N-$Cl_{0.5}(NO_3)_{0.5}$-CP electrode. X-ray photoelectron spectroscopy (XPS) experiments were performed on an XPS instrument (ESCALab250x, Thermo Fisher) and an Al Kα source. In addition, all XPS data were fitted on the C1s line of 284.8 eV according to the intelligent fitting method.

### 1.4 Electrochemical measurement

All electrochemical measurements were performed on the CHI 760E workstation (ChenHua Instrument, Shanghai, China) with a typical three-electrode system in 1 M KOH solution. The Pt gauze electrode, Ag/AgCl electrode, and CP (0.5*0.5 $cm^2$ and 1*1 $cm^2$) were used as the counter electrode, reference electrode, and working electrode, respectively. All measured potentials were calibrated to the reversible hydrogen electrode (RHE) by the following formula:

$$E_{RHE} = E_{Ag/AgCl} + 0.197 + 0.059*pH$$

The linear scanning voltammetry (LSV) curves were tested at room temperature in 1 M KOH solution, while the test voltage range and scanning rate were 0-0.8 V and 5 mV $s^{-1}$, respectively.

In addition, 90% iR compensation and stirring were also required during the test. The Tafel slopes were obtained from the LSV curves.

Cyclic voltammetry (CV) curves were also tested at room temperature and 1 M KOH solution without iR compensation and stirring. In addition, the scanning rates were 1, 5, 25, 50, 75, and 100 mV $s^{-1}$, respectively. The electrochemical impedance spectroscopy (EIS) was carried out from 0.01 to 10000 Hz at the open-circuit potential. Note that the corresponding inherent resistance of the electrolyte, the charge transfer resistance ($R_{ct}$) of the electrode, and the constant phase angle element (CPE) were analyzed by the complex nonlinear least-squares fitting method. Chronopotentiometry of $NiFe_{0.05}$-N-$Cl_{0.5}(NO_3)_{0.5}$-CP with a geometric area of 0.25 $cm^2$ was performed at a constant potential of 1.65 V.

## 2 Supplementary Figures and Tables

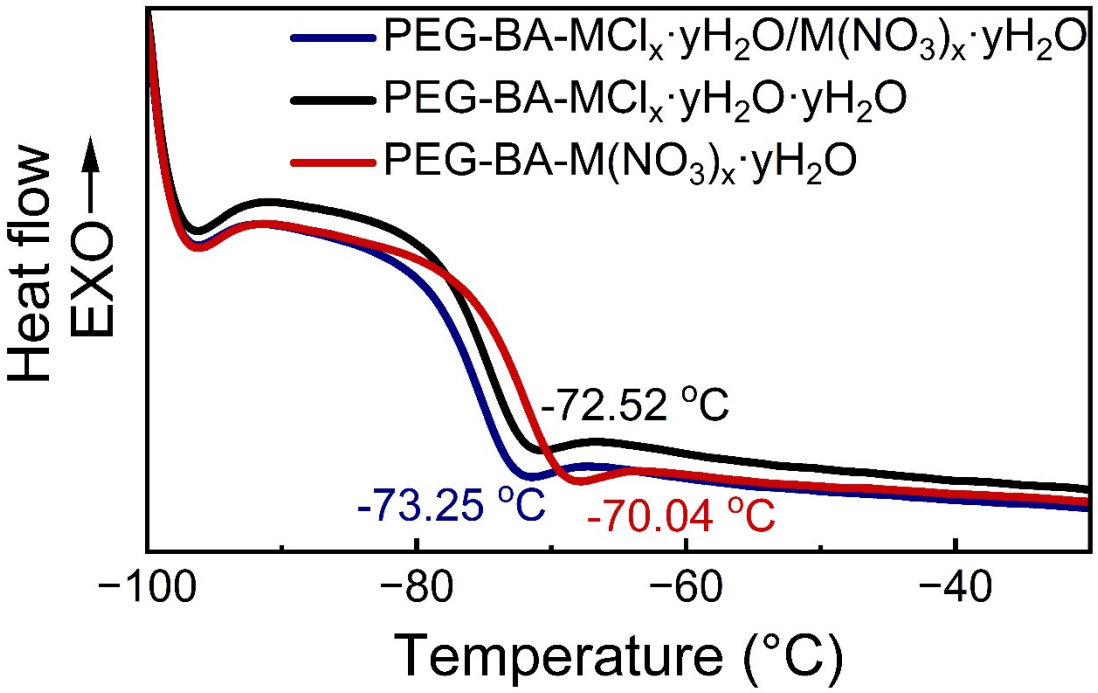


**Fig. S1** DSC curve of the synthesized PEG-BA-MCl$_x$·yH$_2$O, PEG-BA-MCl$_x$·yH$_2$O/ M(NO$_3$)$_x$·yH$_2$O, PEG-BA-M(NO$_3$)$_x$·yH$_2$O.

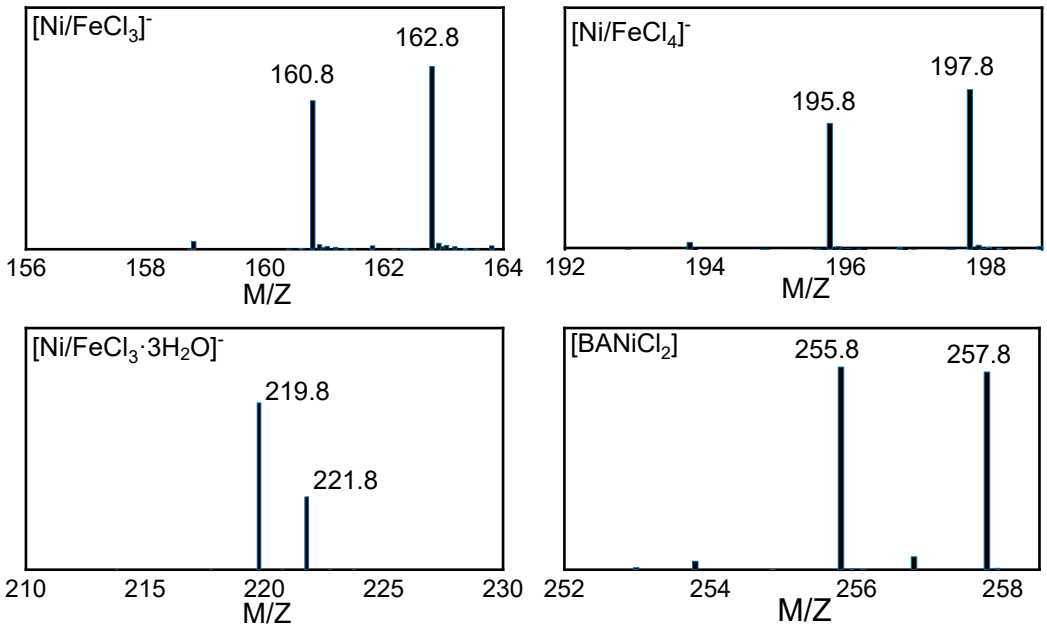


**Fig. S2** Magnified ESI-HRMS spectra of PEG-BA-$NiFe_{0.05}$-Cl DES.

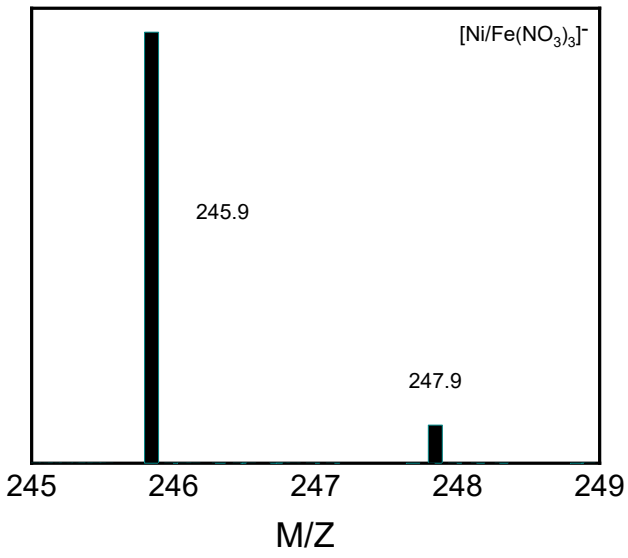


**Fig. S3** Magnified ESI-HRMS spectra of PEG-BA-$NiFe_{0.05}$-$NO_3$ DES.

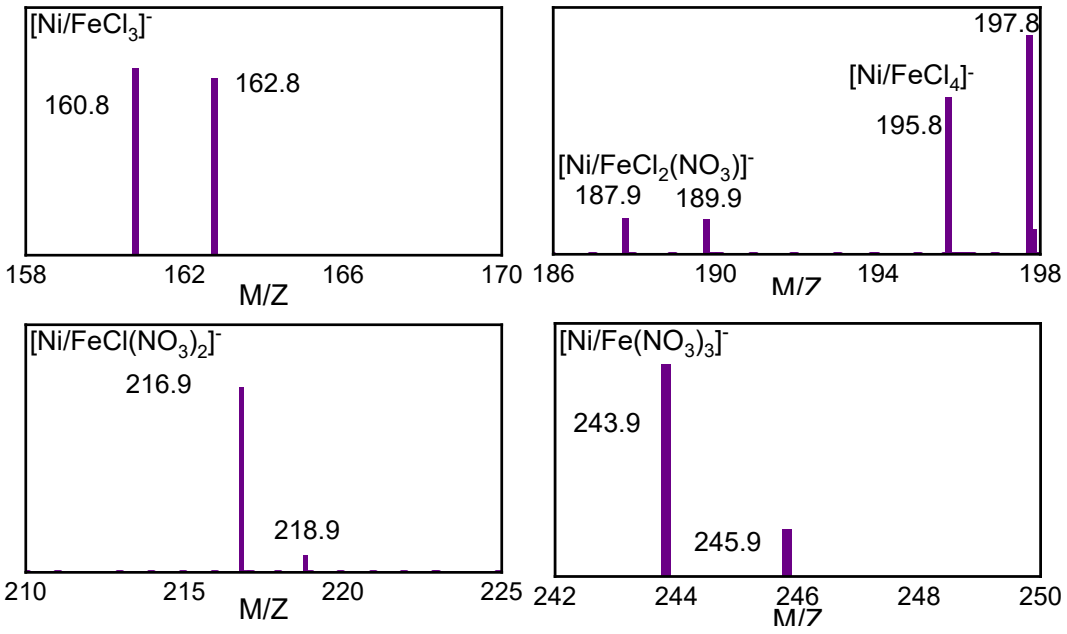


**Fig. S4** Magnified ESI-HRMS spectra of PEG-BA-$NiFe_{0.05}$-$(NO_3)_{0.5}(Cl)_{0.5}$ DES.

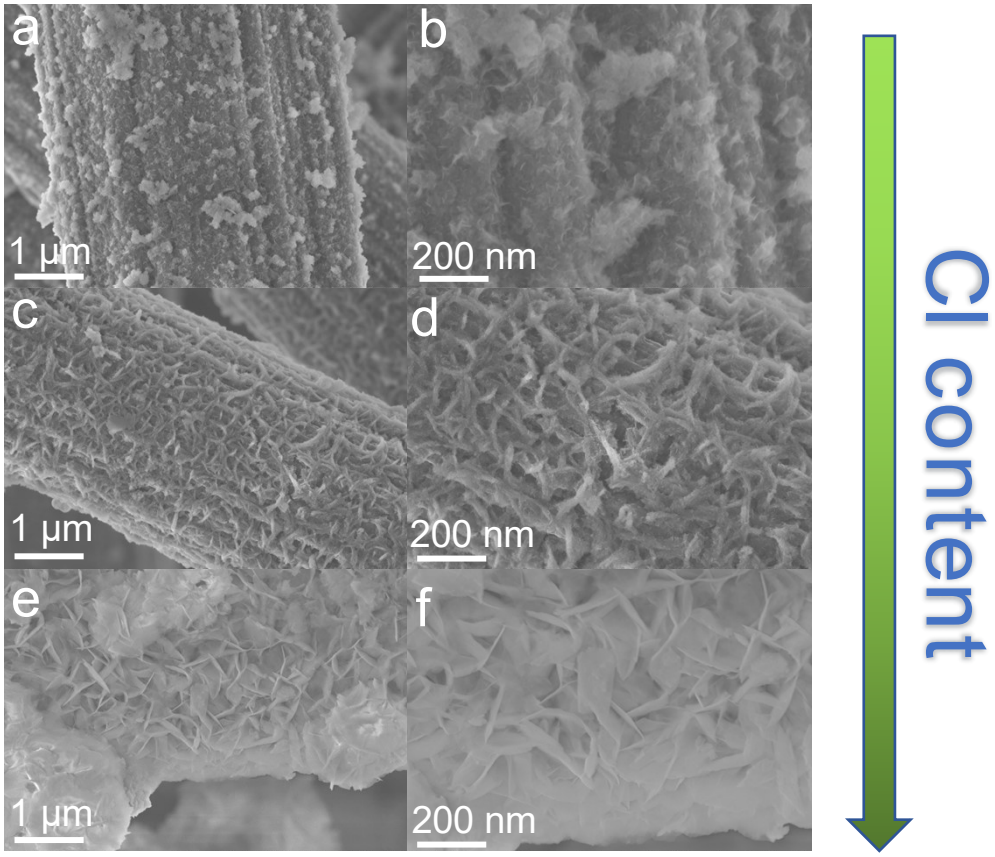


**Fig. S5** SEM images of $NiFe_{0.05}$-N-$NO_3$-CP (a, b); $NiFe_{0.05}$-N-$Cl_{0.5}(NO_3)_{0.5}$-CP (c, d); $NiFe_{0.05}$-N-Cl-CP (e, f).

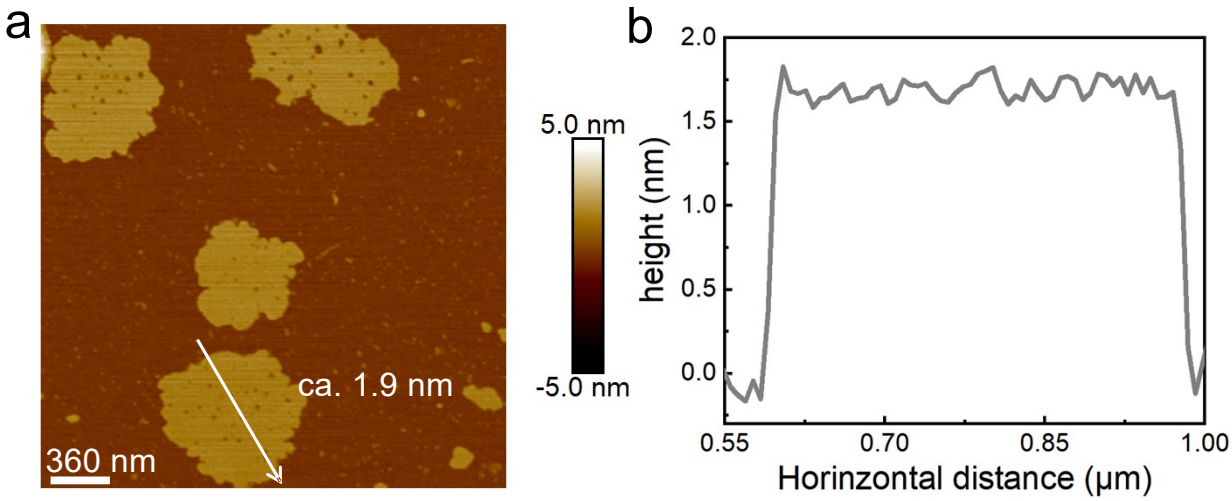


**Fig. S6** AFM image (a) and the corresponding height profile (b) of $NiFe_{0.05}$-N-$Cl_{0.5}(NO_3)_{0.5}$-CP.

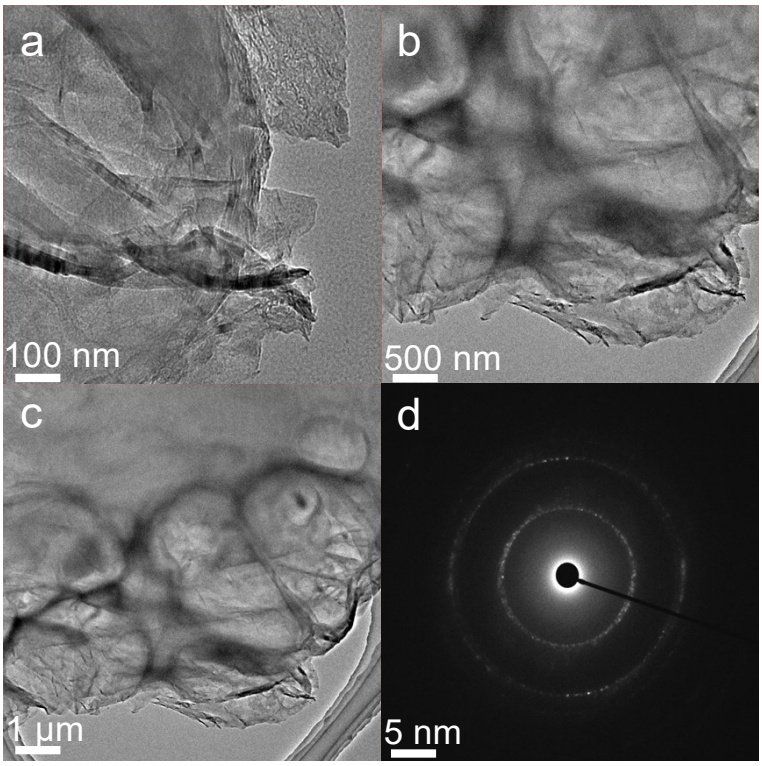


**Fig. S7** (a-c) TEM images and (d) SAED pattern of 2D $NiFe_{0.05}$-N-$Cl_{0.5}(NO_3)_{0.5}$.

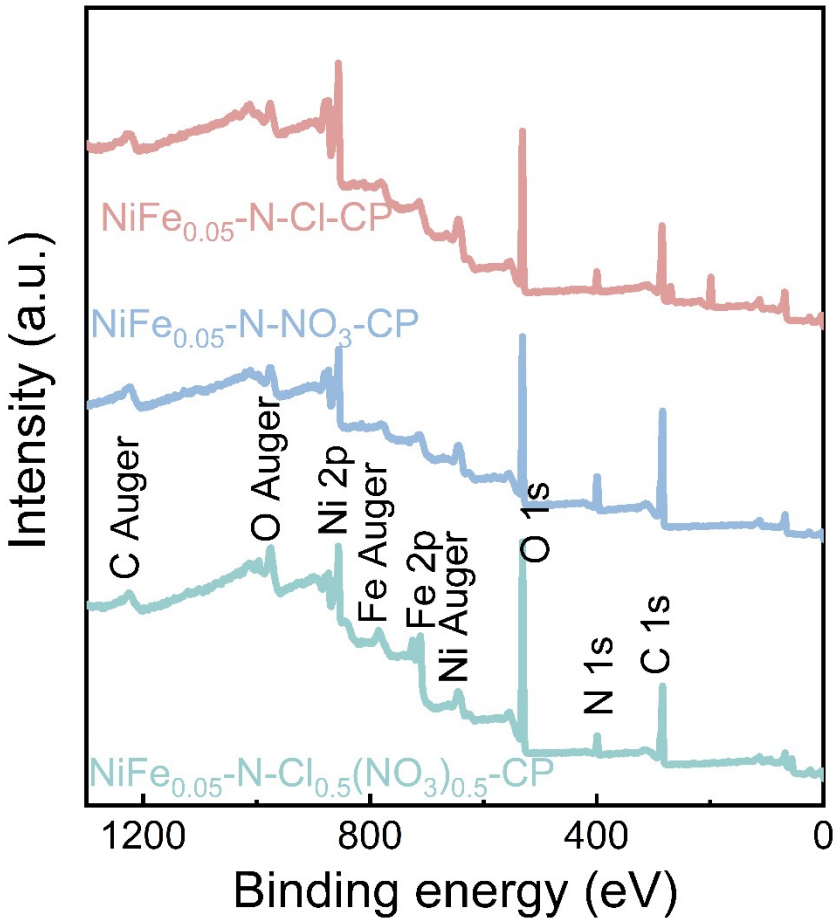


**Fig. S8** The full XPS survey spectra of $NiFe_{0.05}$-N-Cl-CP, $NiFe_{0.05}$-N-$NO_3$-CP, and $NiFe_{0.05}$-N-$Cl_{0.5}(NO_3)_{0.5}$-CP.

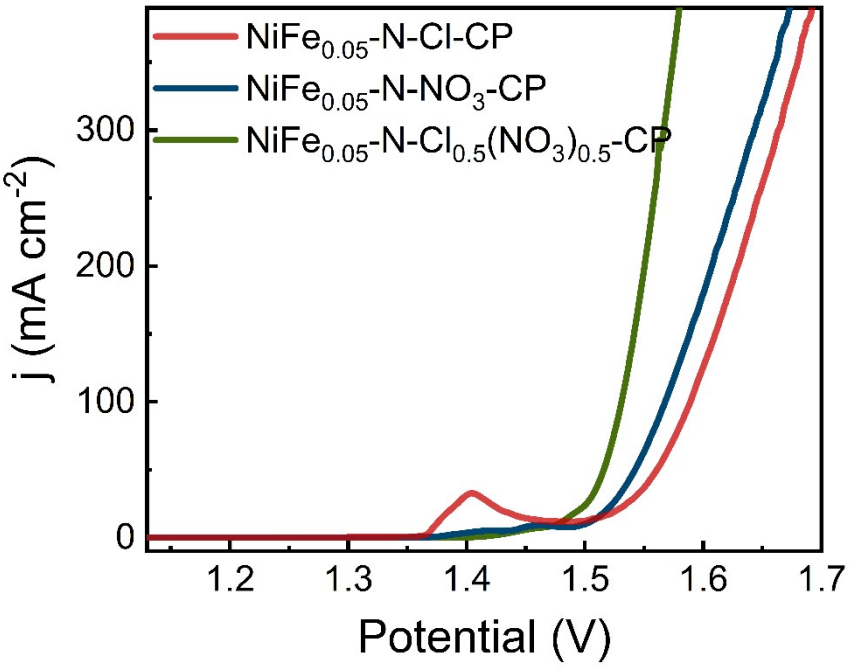


**Fig. S9** LSV curves of $NiFe_{0.05}$-N-Cl-CP, $NiFe_{0.05}$-N-$NO_3$-CP, and $NiFe_{0.05}$-N-$Cl_{0.5}(NO_3)_{0.5}$-CP at first cycle.

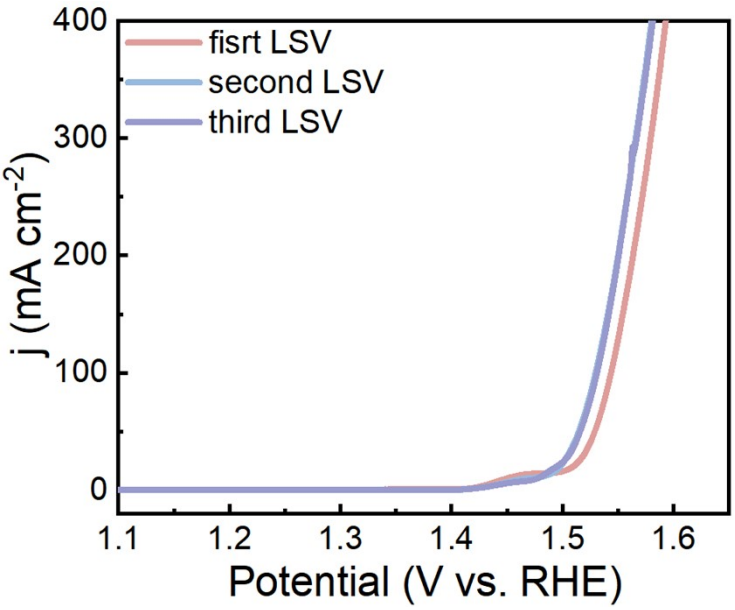


**Fig. S10** LSV curves of $NiFe_{0.05}$-N-$Cl_{0.5}(NO_3)_{0.5}$-CP with different cycles.

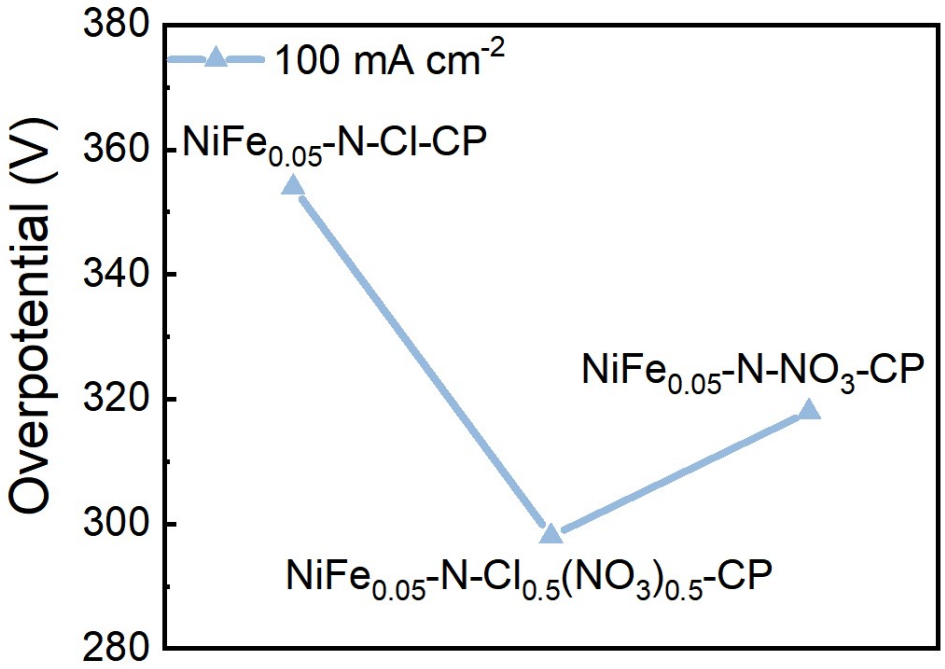


**Fig. S11** Overpotential values of $NiFe_{0.05}$-N-Cl-CP, $NiFe_{0.05}$-N-$Cl_{0.5}(NO_3)_{0.5}$-CP, and $NiFe_{0.05}$-N-$NO_3$-CP.

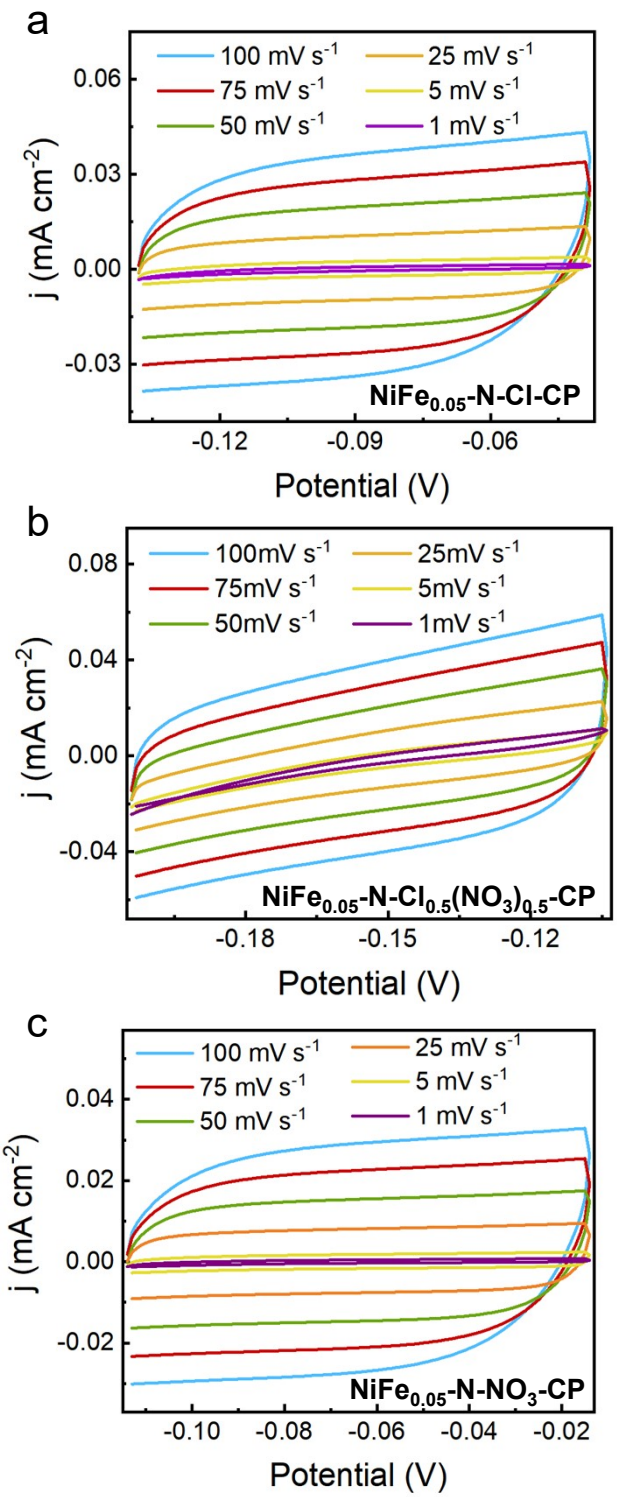


**Fig. S12** CV curves of (a)$NiFe_{0.05}$-N-Cl-CP, (b) $NiFe_{0.05}$-N-$Cl_{0.5}(NO_3)_{0.5}$-CP, and (c) $NiFe_{0.05}$-N-$NO_3$-CP at different scan rates ranging from 1 to 100 mV $s^{-1}$.

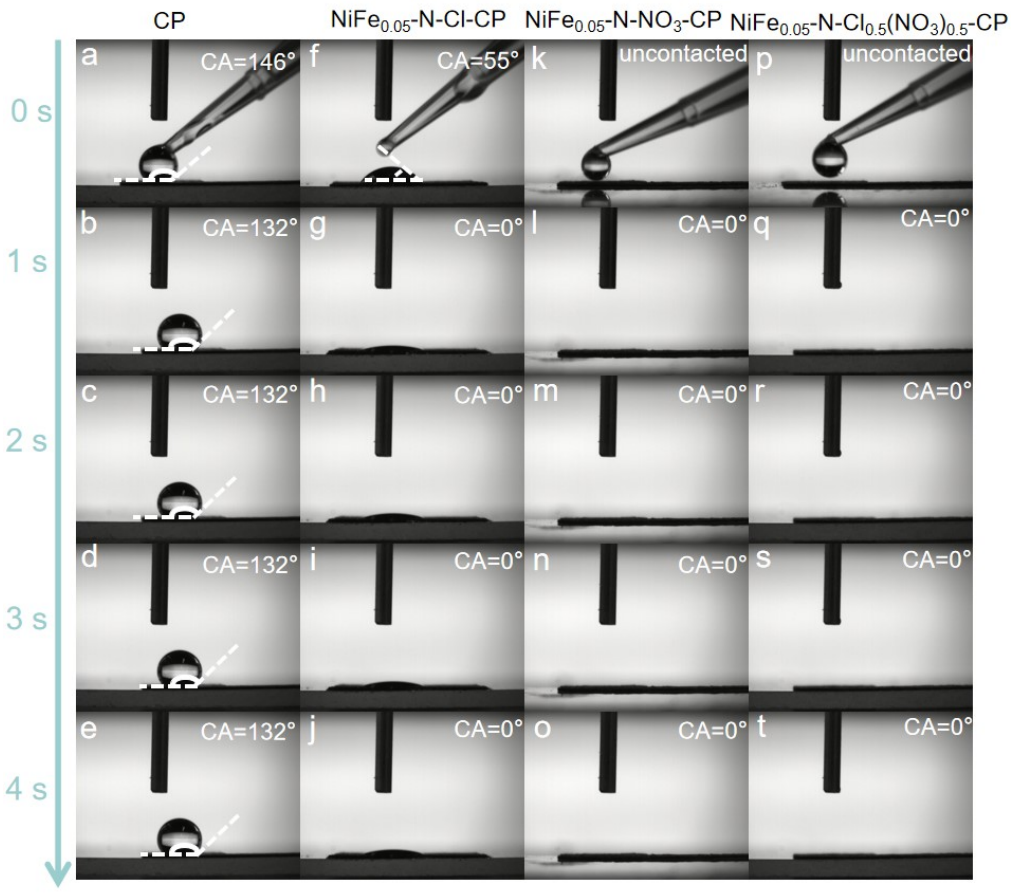


**Fig. S13** Static water droplet contact angles of CP, $NiFe_{0.05}$-N-Cl-CP, $NiFe_{0.05}$-N-$Cl_{0.5}(NO_3)_{0.5}$-CP and $NiFe_{0.05}$-N-$NO_3$-CP.

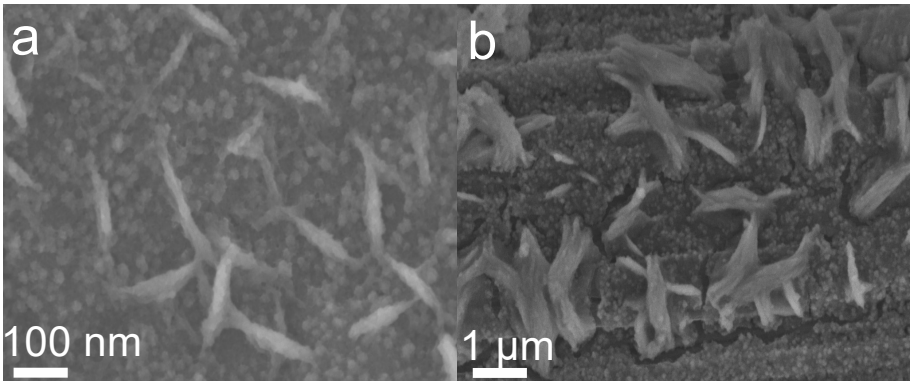


**Fig. S14** SEM images of $NiFe_{0.05}$-N-$Cl_{0.5}(NO_3)_{0.5}$-CP after OER cycling.

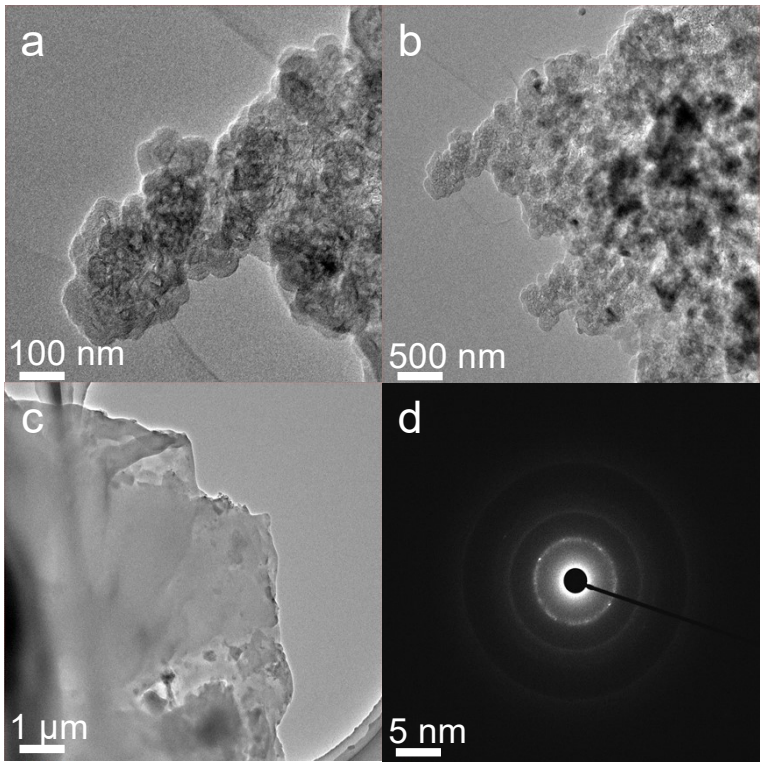


**Fig. S15** (a-c) TEM images and (d) SAED pattern of $NiFe_{0.05}$-N-$Cl_{0.5}(NO_3)_{0.5}$-CP after OER cycling.

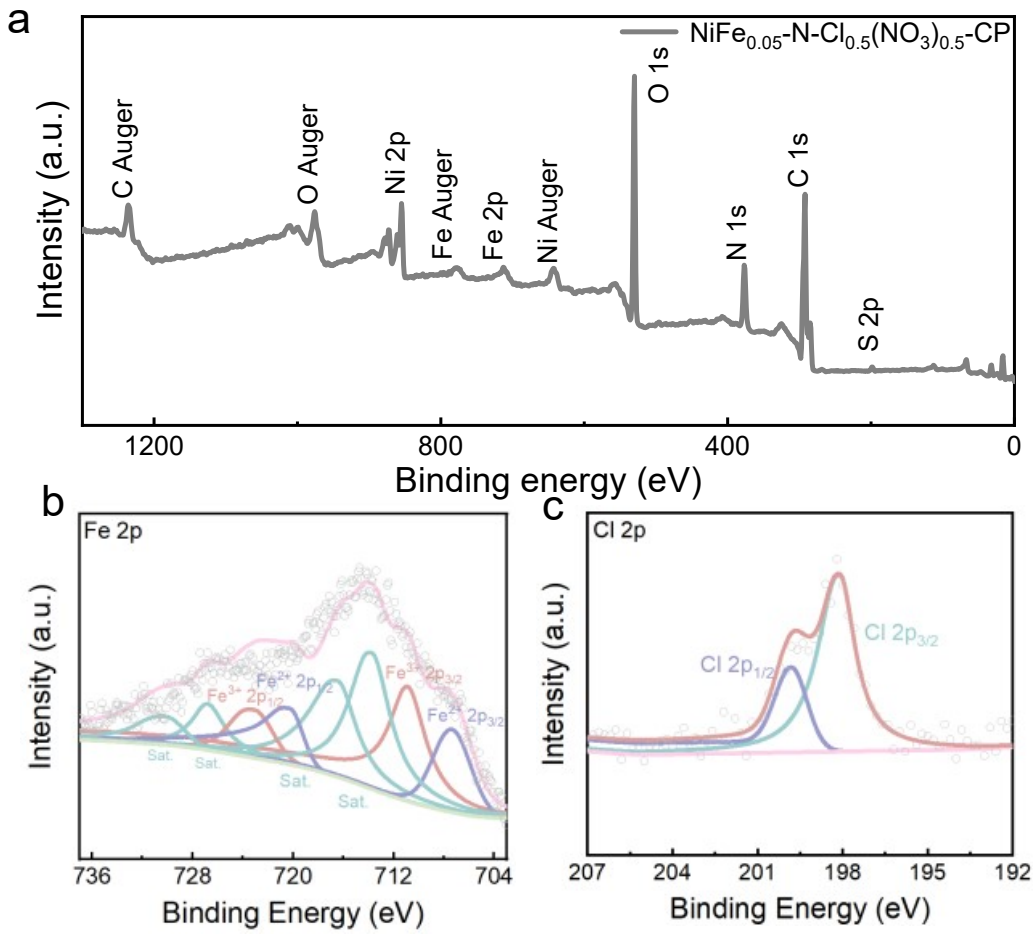


**Fig. S16** (a) The full, High-resolution (b) Fe 2p, and (c) Cl 2p XPS spectra of $NiFe_{0.05}$-N-$Cl_{0.5}(NO_3)_{0.5}$-CP after OER cycling.

**Table S1** OER performance of the prepared NiFe nitrides and other representative reported non-precious metal electrocatalysts in the alkaline media.

| catalysts | Current density (mA $cm^{-2}$) | Overpotential (mV) | Reference |
|---|---|---|---|
| $NiFe_{0.05}$-N-Cl-CP | 100 | 354 | *This work* |
| **$NiFe_{0.05}$-N-$Cl_{0.5}(NO_3)_{0.5}$-CP** | **100** | **298** | ***This work*** |
| $NiFe_{0.05}$-N-$NO_3$-CP | 100 | 318 | *This work* |
| $CoMoN_x$ | 10 | 290 | *[1]* |
| $W_2N$ | 10 | 222 | *[2]* |
| VN/WN@NC | 10 | 122 | *[3]* |
| P-NCO/NCN-CF@CC | 10 | 349 | *[4]* |
| Co-NC@$Mo_2C$ | 10 | 347 | *[5]* |
| NiCoN/CNT | 10 | 280 | *[6]* |
| $NiFe_2O_4$ | 50 | 280 | *[7]* |
| NiCoHPi@$Ni_3N$/NF | 100 | 365 | *[8]* |
| MoN-$Co_2N$/NF | 100 | 357 | *[9]* |
| NiFeN | 100 | 307 | *[10]* |
| NiFeN@C/NF | 100 | 314 | *[11]* |
| Co/$Co_4N$@NC | 100 | 408 | *[12]* |
| NiTe-NiFeN | 400 | 350 | *[13]* |
| $Fe_2P$/$Ni_3N$ | 500 | 252 | *[14]* |
| NiMoN/NiFe LDH | 1000 | 266 | *[15]* |
| $NiFe_{0.05}$-N | 100 | 320 | *[16]* |
| $La_{0.5}Sr_{0.5}Co_{0.8}Fe_{0.2}O_3$ | 10 | 304 | *[17]* |
| CoMnO | 10 | 300 | *[18]* |

**Table S2** $C_{dl}$ and $R_{ct}$ values of the obtained self-supporting electrodes.

| **electrodes** | **$C_{dl}$ (μF cm$^{-2}$)** | **$R_{ct}$ (Ohm)** |
|---|---|---|
| $NiFe_{0.05}$-N-Cl-CP | 349.0 | 10.0 |
| $NiFe_{0.05}$-N-$Cl_{0.5}(NO_3)_{0.5}$-CP | 387.0 | 3.2 |
| $NiFe_{0.05}$-N-$NO_3$-CP | 282.0 | 7.5 |

## 3 References


1 Y. Lu, Z. Li, Y. Xu, L. Tang and S. Xu, *Chem. Eng. J.*, 2021, **411**, 128433.

2 Z. Hong, Z. Xu, Z. Wu, H. Zhang, P. Li, X. Xu and S. Duo, *Appl. Surf. Sci.*, 2023, **6081**, 55159.

3 D. He, L. Cao, J. Huang, S. Li, Y. Feng, G. Li, F. Wang and L. Feng, *Chem. Eng. J.*, 2022, **429**,131945.

4 Y. Liu, Z. Jiang, Z. Jiang, *Adv. Funct. Mater.*, 2023, **33**, 2302883.

5 M. You, X. Du, X. Hou, Z. Wang, Y. Zhou, H. Ji, L. Zhang and D. Chen, *Appl. Catal. B*, 2022, **317**, 121729.

6 X. Chen, X. Yu, G. Zhang, Y. Huang, H. Wang, J. Jiang, Z. Ma and Q. Li, *J. Electroanal. Chem.*, 2024, **958**, 118162.

7 X. Wang, Z. Jiang, Y. Ma, X. Su, X. Zhao, A. Zhu and Q. Zhang, *J. Power Sources*, 2024, **591**, 233819.

8 H. Sun, J. Sun, X. Tian, C. Li and L. Zhang, *ACS Appl. Mater. Interfaces*, 2022, **14**, 22061.

9 X. Wang, X. Han, R. Du, C. Xing, X. Qi, Z. Liang, P. Guarida, J. Arbiol, A. Cabot and J. LiACS, *ACS Appl. Mater. Interfaces*, 2022, **14**, 41924.

10 L. Yu, Q. Zhu, S. Song, B. McElhenny, D. Wang, C. Wu, Z. Qin, J. Bao, Y. Yu, S. Chen and Z. Ren, *Nat. Commun.*, 2019, **10**, 5106.

11 B. Wang, M. Lu, D. Chen, Q. Zhang, W. Wang, Y. Kang, Z. Fang, G. Pang and S. Feng, *J. Mater. Chem. A*, 2021, **9**, 13562.

12 H. Choi, J. Kim, H. Bang, K. Badawy, N. Singh and D. Yoon, *J. Mater. Chem. A*, 2024, **12**, 45.

13 R. Li, Y. Li, P. Yang, P. Ren, D. Wang, X. Lu, R. Xu, Y. Li, J. Xue, J. Zhang, M. An, J. Ma, B. Wang, H. Liu and S. Dou, *Appl. Catal. B*, 2022, **318**, 121834.

14 W. Ma, D. Li, L. Liao, H. Zhou, F. Zhang, X. Zhou, Y. Mo and F. Yu, *Small*, 2023, **19**, 2207082.

15 P. Zhai, C. Wang, Y. Zhao, Y. Zhang, J. Gao, L. Sun and J. Hou, *Nat. Commun.*, 2023, **14**, 37015944.

16 Y. Xu, Z. Cheng, J. Jiang, J. Du and Q. Xu, 2021, *Chem. Commun.*, 2021, **57**, 13170.

17 K. Rong, J. Wei, L. Huang, Y. Fang and S. Dong, *Nanoscale.*, 2020, **12**, 20719.

18 A. Samage, K. Pramoda, M. Halakarni and N. Kotrappanavar, *ACS Appl. Energy Mater.*, 2023, **6**, 2412-2422.